

Microcavity Electrodes Used as Single-Nucleation Site Electrodes for the Electrolysis of Water

Alexandru Volanschi, Joanne G. H. Nijman,¹
Wouter Olthuis² and Piet Bergveld²

Unilever Research Laboratory, P. O. Box 114, 3130 AC, Vlaardingen, The Netherlands

¹Vita tron, P. O. Box 76, 6950 AB Dieren, The Netherlands

²MESA Research Institute, University of Twente
P. O. Box 217, 7500 AE Enschede, The Netherlands

(Received February 22, 1996; accepted February 12, 1997)

Key words: metal electrode, electrolysis, gas bubble nucleation, surfactant, dynamic surface tension

In this paper, we report controlled gas bubble formation during electrolysis by means of electrode surface shaping in the form of microcavity electrodes (MCEs). A theoretical model is given to support the concept of using electrode surface shaping for obtaining reproducible nucleation of gas bubbles during electrolysis. The gas bubble evolution process is monitored by simultaneous measurement of overpotential and impedance fluctuations. The reproducibility of the nucleation process at the MCEs is shown in terms of a constant bubble frequency. A qualitative model is proposed to explain the shape of the measured waveforms. The possible use of the MCE device as a surface tension sensor with a frequency output is recognized.

1. Introduction

Gas evolution reactions at metal electrodes during electrolysis processes have been thoroughly reported in a number of publications. The attention of most authors has been focused mainly on mass transfer processes, the reaction kinetics at gas-evolving electrodes and on various components of overpotential during the gas evolution reaction. Macroelectrodes as well as microelectrodes were used in those studies. A diverse variety of applications has been proposed, ranging from mass transfer enhancement by local

stirring^(1,2) to industrial electrolysis processes⁽³⁾ and dynamic surface tension measurements.⁽⁴⁾

Investigations into the nucleation processes of gas phases in liquids have also been published. It is generally accepted that nucleation takes place in natural cavities (natural nucleation sites) randomly distributed over the surface of the electrode. Few publications deal with artificial nucleation sites for gas-evolving electrodes, and those which do concern nucleated pool boiling.⁽⁵⁾ No reference can be found in publications in which artificial nucleation sites for reproducible single bubble generation are used during electrolysis. Microelectrodes were not considered as artificial nucleation sites since, although the number of natural nucleation sites can be reduced by reducing the electrode size, the nucleation still cannot be controlled. One method for obtaining more information about the nucleation processes is the stochastic approach.⁽⁶⁾ This approach is based on a previously reported spectral analysis method.⁽⁷⁾ Another approach to the difficulty is to create a nucleation site where monosized bubbles nucleate and grow in a controlled manner. The advantage is that this enables investigation of single bubbles. Although a single nucleation site electrode can be produced, the nature of the bubble nucleation process during electrolysis must be understood before such an artificial nucleation site can be optimized. To facilitate the nucleation of gas bubbles, the liquid must first be supersaturated with dissolved gas. The actual value of supersaturation needed for heterogeneous nucleation is strongly dependent on other parameters such as the state of the electrode surface, the type of electrode material, surface tension and the chemical composition of the liquid.

Nucleation of gas bubbles in liquids can occur through different mechanisms. One possibility is homogeneous nucleation, whereby bubbles appear in the bulk of the mother phase in places where the influence of any interface in the system is negligible. The driving force during the homogeneous nucleation is the excess in chemical potential of the liquid phase as compared with that of the gas. Return to a stable situation results in the formation of a bubble. The conditions for homogeneous nucleation are rarely met, which is why homogeneous nucleation is not as practically significant as heterogeneous nucleation.

Gas bubbles are formed at the surface of an electrode or at a wall of the containing vessel by heterogeneous nucleation. The driving force is still the chemical potential, but the presence of the wall plays an important role through the contact angle. The contact angle is defined as the angle of the liquid-gas interface to the solid-liquid interface at the three phase contact point. For a nonzero contact angle, heterogeneous nucleation is energetically preferred to homogeneous nucleation.⁽⁶⁾ In the limiting case where the contact angle is zero, heterogeneous nucleation ceases to have any energetic advantage over homogeneous nucleation. In the particular case of electrolysis, gas supersaturation is always higher at the electrode-liquid interface than in the bulk liquid because the gas is generated at the electrode surface. Due to this nonuniform concentration profile and the fact that bubbles nucleate in regions in which supersaturation is high, bubbles will nucleate at the electrodes and not in the bulk of the liquid electrolyte. Note that both homogeneous and heterogeneous nucleation mechanisms imply that the gas phase did not exist before nucleation.

Another possibility for the formation of bubbles in a liquid is to start from an existing bubble source in the form of *traces of gas* (i.e., to continue the growth of the existing gas

phase). These traces of gas, called Harvey nuclei,⁽⁸⁾ may be present in pockets (small cavities) on the surface of an electrode or the wall of the containing vessel and are in equilibrium with the environment. If the concentration of dissolved gas exceeds a maximum value, depending on the dimensions of the pockets, the corresponding Harvey nucleus becomes active and a bubble will grow from that pocket.

On any existing flat electrode, the position where bubbles nucleate is unknown and independent of the active nucleation mechanism. Miniaturization of the electrode to the same order of size as the bubble seems to be one solution for fixing the nucleation site. However, even on such small flat microelectrodes, bubbles might form at random places in an uncontrolled manner. Two bubbles can nucleate at the same time and remain so small that they do not coalesce.⁽⁹⁾ The previously used microelectrode was made from a platinum wire sealed in glass and had a diameter of 127 μm (0.005 in.). Gabrielli *et al.*⁽¹⁰⁾ obtained single bubbles from flat microelectrodes with comparable dimensions (100 μm diameter). The difference in results is possibly due to the different experimental conditions or to a different electrode polishing procedure. The reproducibility of the nucleation of single bubbles from flat electrodes has thus not yet been demonstrated.

The bubble evolution can be monitored optically using a microscope and various image recording techniques, as well as electrically.⁽¹⁰⁾ Electrical monitoring is based on the fact that the electrode surface area in contact with the liquid solution fluctuates during the bubble evolution process, which induces fluctuations in the electrode overpotential and in electrode impedance. Additional processing of the signals by means of spectral analysis can also be considered.⁽⁷⁾ Various models describing the overpotential and impedance variations at electrodes can be found in the literature.^(6,11,12) Several aspects can be taken into account to create a model of the influence of bubble evolution due to electrolysis on the overpotential. The complexity of the model increases as more effects are considered.⁽¹³⁾ Each effect is responsible for one component of the overpotential, i.e., ohmic losses due to the presence of bubbles, surface potential due to irreversible electrode reaction, concentration overpotential of dissolved gas and concentration overpotential due to ions. Measurements of overpotential were published in ref. 10 and simultaneous measurements of overpotential and impedance in ref. 11. Several bubbles evolved at the same time in the processes described in ref. 11 and therefore no information about the nucleation of single bubbles can be obtained.

In this paper, we further investigate the heterogeneous nucleation process. Artificial nucleation sites in the form of microcavity electrodes (MCEs) are proposed for the control of heterogeneous nucleation of gas bubbles. An example of a cavity with edge length h embedded in a plane is shown in Fig. 1. It is shown that the cavity acts as a concentrator, which means that a more pronounced concentration nonuniformity is expected on the bottom of the MCE than at the surface of a flat electrode. Consequently, heterogeneous nucleation is expected to take place on the bottom of the cavity. A simplified analytical model is given to support the experimental evidence of the concentrator effect of the microcavity electrodes. The bubble detection was performed by monitoring the fluctuations of either the electrode overpotential or the electrode impedance using a method similar to that of Gabrielli *et al.*⁽¹¹⁾

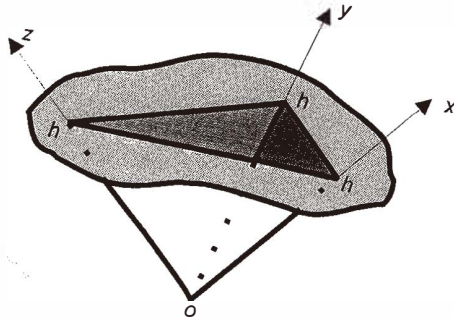


Fig. 1. Schematic of a microcavity with edge length h embedded in a plane.

2. Theory

It is necessary to give a theoretical basis for the assumption that gas bubble nucleation during electrolysis takes place first on the bottom of a MCE. This nucleation appears as a consequence of the concentrator effect and a heterogeneous nucleation mechanism. It must be emphasised that the model is thought to describe the evolution of the concentration profile before the formation of a gas phase at the electrode and not after a bubble has started to grow. As an example, the electrolysis of water was considered, but the results are, in principle, valid for any other electrolysis. Consequently, the gas evolving at the MCE is either hydrogen or oxygen. Due to electrolysis, the concentration of dissolved gas at the electrode surface is higher than in the bulk electrolyte, and the gas molecules will diffuse from the electrode to the bulk of the solution.

Solving this diffusion problem in the general three-dimensional case is very difficult. Some simplifying assumptions must be made. The cavity is assumed to consist of three plane electrodes perpendicular to each other (Fig. 2). Away from the common intersection point ($x, y, z = 0$), the electrodes are assumed to be infinitely extended. No migration or convection will be considered. Diffusion of species is possible only at a point perpendicular to the surface of the electrode. Even with such a highly simplified model, the essence of the concentrator effect of the microcavity can be established. With all these assumptions the diffusion equation for the three-dimensional electrode becomes

$$\frac{\partial C(x, y, z, t)}{\partial t} = D \left(\frac{\partial^2 C(x, y, z, t)}{\partial x^2} + \frac{\partial^2 C(x, y, z, t)}{\partial y^2} + \frac{\partial^2 C(x, y, z, t)}{\partial z^2} \right) \quad (1)$$

$$x, y, z \geq 0,$$

where $C(x, y, z, t)$ is the concentration of dissolved gas at point (x, y, z) and at time t and D is the diffusion coefficient of the dissolved gas molecules.

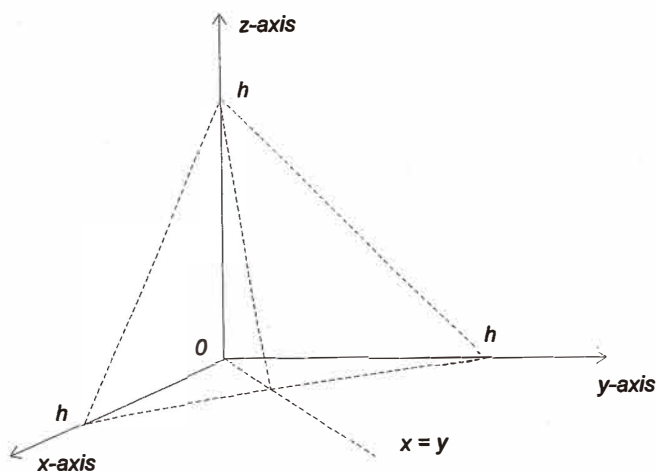


Fig. 2. Schematic of a three-dimensional cavity electrode where the electrode planes are perpendicular to each other.

As an initial condition (at $t = 0$), it is assumed that the concentration of dissolved gas in the whole solution ($x, y, z > 0$) is zero.

$$C(x, y, z, 0) = 0 \quad (2)$$

It is also assumed that the current through the MCE, i , is uniformly distributed over the whole electrode area, A . The plane electrodes produce gas at a constant rate k due to a constant current density ($J = i/A$):

$$\frac{\partial C(0, y, z, t)}{\partial x} = -\frac{s_g J}{z_e DF} = -k \quad (3)$$

$$\frac{\partial C(x, 0, z, t)}{\partial y} = -\frac{s_g J}{z_e DF} = -k \quad (4)$$

$$\frac{\partial C(x, y, 0, t)}{\partial z} = -\frac{s_g J}{z_e DF} = -k, \quad (5)$$

where F is the Faraday constant, s_g is the stoichiometric coefficient and z_e is the number of electrons involved in the gas evolution reaction. For the hydrogen evolution reaction, $s_g/z_e = 1/2$.

As a last boundary condition, it may be assumed that at an infinite distance from the electrode, and at any time, the influence of the electrode will not be felt. The distance to the

electrode planes is infinite if all the space coordinates are infinite:

$$\lim_{x,y,z \rightarrow \infty} C(x, y, z, t) = 0. \quad (6)$$

Because there is a steady flow from the three electrode planes, $\frac{\partial C}{\partial n} = -k$, $n = x, y, z$, the solution to the diffusion problem can be written as a superposition of simple results.⁽¹⁴⁾ We assume a configuration like that in Fig. 2, but where only the xy plane is an electrode and the xz and yz planes are diffusion-impermeable plates. The initial condition (eq. (2)) will remain unchanged. The impermeable xz and yz plates lead to new boundary conditions:

$$\frac{\partial C(x, 0, z, t)}{\partial y} = \frac{\partial C(0, y, z, t)}{\partial y} = 0. \quad (7)$$

The boundary condition at the xy plane will remain unchanged (eq. (5)). The solution to the one-dimensional case in the z direction satisfying the diffusion equation (eq. (1)) and the initial and boundary conditions (eq. (2), (5)–(7)) is

$$C(x, y, z, t) = k \left(2\sqrt{\frac{Dt}{\pi}} \exp\left(\frac{-z^2}{4Dt}\right) - z \cdot \operatorname{erfc}\left(\frac{z}{2\sqrt{Dt}}\right) \right). \quad (8)$$

According to the uniqueness theorem,⁽¹⁵⁾ the solution found is also the only possible solution to the problem with one plane electrode and two impermeable plates, all perpendicular to each other.

Similar solutions can be deduced for the case in which the xz and yz planes are used as electrodes. Superposition of the solutions to the problems with one electrode and two impermeable plates leads to the solution of the problem with three electrodes:

$$C(x, y, z, t) = k \left(2\sqrt{\frac{Dt}{\pi}} \exp\left(\frac{-x^2}{4Dt}\right) - x \cdot \operatorname{erfc}\left(\frac{x}{2\sqrt{Dt}}\right) \right) + k \left(2\sqrt{\frac{Dt}{\pi}} \exp\left(\frac{-y^2}{4Dt}\right) - y \cdot \operatorname{erfc}\left(\frac{y}{2\sqrt{Dt}}\right) \right) + k \left(2\sqrt{\frac{Dt}{\pi}} \exp\left(\frac{-z^2}{4Dt}\right) - z \cdot \operatorname{erfc}\left(\frac{z}{2\sqrt{Dt}}\right) \right). \quad (9)$$

It is proved in the appendix that solution (9) satisfies the diffusion equation (eq. (1)) and the boundary and initial conditions (2)–(6). A concentration profile can be represented on the cross section defined by the $(x=y)z$ plane (Figs. 2 and 3). Such a plot was derived using MATLAB (version 4.2c1, The Math Works, Inc.) and is shown in Fig. 4. The concentra-

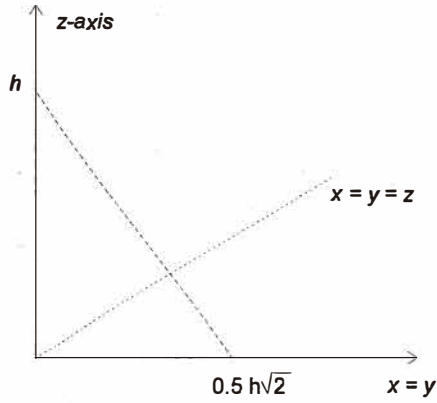


Fig. 3. Cross section of the cavity in Fig. 1 on the $x = y$ plane.

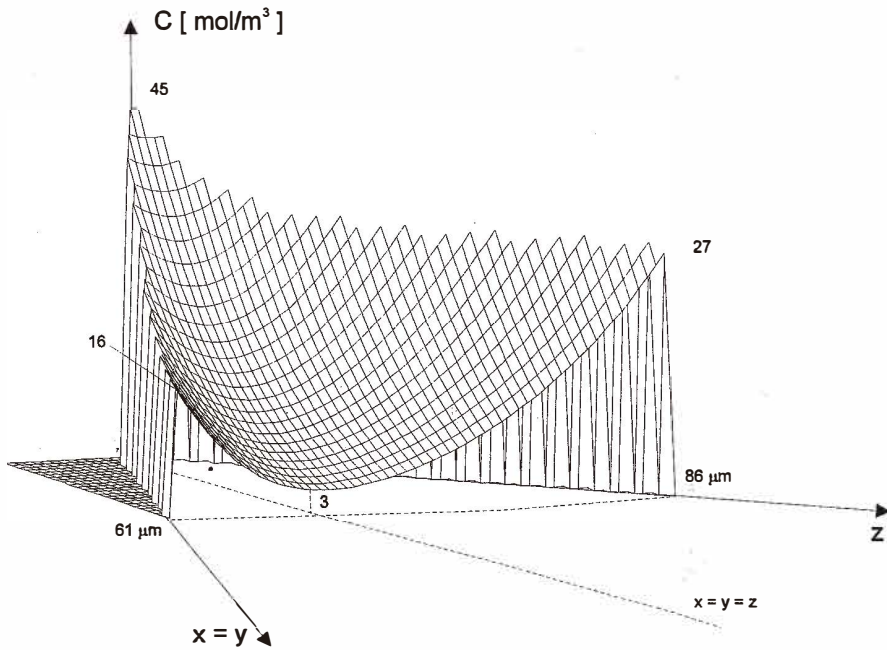


Fig. 4. Concentration profile of three electrodes perpendicular to each other. The concentration profile corresponds to the cross section in Fig. 3 ($t = 0.1$ s, $J = 500$ Am⁻², $D = 3.5 \times 10^{-9}$ m²s⁻¹⁽²⁾).

tion profile is represented as various heights with respect to the $(x=y)z$ plane. Because the cross section on the $(x=y)z$ plane in the three-dimensional cavity is not symmetric with respect to the line $x = y = z$, the concentration profile has an asymmetric form. The maximum of the concentration profile, corresponding to a maximum supersaturation of produced gas, is found at the bottom of the cavity at $(x,y,z) = (0,0,0)$.

Suppose the time τ_i is the time elapsed until a certain supersaturation is reached on the bottom of the cavity after starting the electrolysis from the initial conditions (eq. (2)), where i refers to the one- or three-dimensional problem. Substitution of the time τ_{3D} and $x = y = z = 0$ into the solution from eq. (9) gives

$$C(0,0,0, \tau_{3D}) = 3 \cdot 2k \cdot \sqrt{\frac{D\tau_{3D}}{\pi}}. \quad (10)$$

Substitution of the time τ_{1D} and $z = 0$ in the solution of the one-dimensional case (eq. (8)) gives

$$C(x,y,0, \tau_{1D}) = 2k \cdot \sqrt{\frac{D\tau_{1D}}{\pi}}. \quad (11)$$

Note that this value of supersaturation will in theory be reached throughout the xy plane, thus also in $x = y = z = 0$.

From eqs. (10) and (11) the relationship between the induction time in the one-dimensional and the three-dimensional cases can be deduced as

$$\tau_{3D} = \frac{1}{9} \tau_{1D}, \quad (12)$$

which shows that the induction time is much shorter in the three-dimensional case than in the case of a planar electrode (one dimensional) for the same current density (same k). The position where the highest supersaturation is reached is also known, in the case of the cavity electrode, to be the bottom of the cavity where $x = y = z = 0$. As a result of the concentrator effect of a MCE, a bubble is expected to nucleate on the bottom of the cavity. Because the nucleation is expected to take place at the electrode surface, a heterogeneous nucleation mechanism is expected.

3. Materials and Methods

3.1 Technology to produce microcavity electrodes

For practical reasons mainly concerning the reproducibility of the fabrication process, the MCEs were made by means of silicon technology. A top and a cross-sectional view of a MCE is presented in Fig. 5.

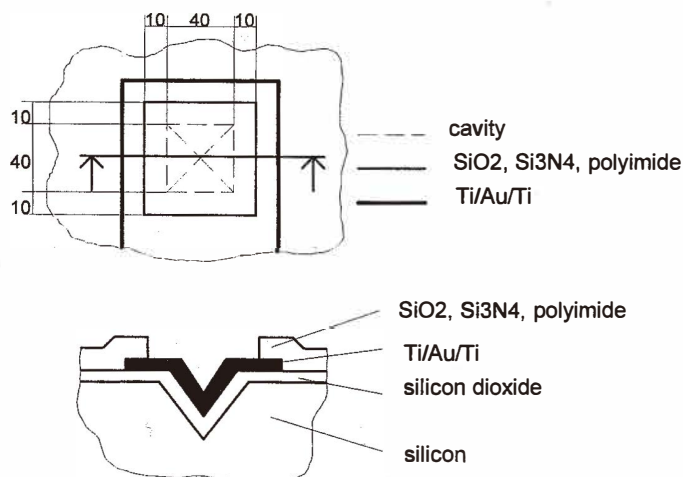


Fig. 5. Schematic of a MCE having a one bubble nucleation site. Top and cross-sectional views. All the dimensions are in μm . The cavity depth is $28.24 \mu\text{m}$.

Silicon wafers with a $\langle 100 \rangle$ crystal orientation were used. The cavities were etched in KOH (33% wt.) through a SiO_2 mask. The advantage of this technique is that pyramidal cavities with reproducible characteristics can be anisotropically etched in silicon. The shape of the structure is a reversed pyramid with a square base. Only the aperture of the cavity can be independently changed, which implies a certain depth of the cavity. Due to silicon batch processing, polishing steps such as those described in ref. 10, which are applied to each electrode independently, are no longer needed. Also, by using this planar process, sealing of a very thin wire in glass is avoided.

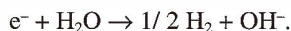
It has been reported^(3,10) that gas bubbles grown by electrolysis on microelectrodes have diameters on the order of $10\text{--}200 \mu\text{m}$. To generate bubbles in a cavity, the aperture of the cavity should be comparable in size with the bubbles. Therefore, the aperture selected was a square with a side length of $40 \mu\text{m}$. The resulting cavity depth was $28.24 \mu\text{m}$.

A sandwich of Ti/Au/Ti with thicknesses of 25/250/25 nm, respectively, was evaporated and patterned on the wafers. The active area of the MCEs was defined with a sandwich of SiO_2 , Si_3N_4 , and photocurable polyimide. At the end of this patterning process, the titanium top layer was removed by chemical etching in hydrofluoric acid solution (HF, 40% Merck, analytical grade, diluted in demineralized water in the proportion 1:10), allowing the gold surface to have a free contact with the aqueous solution. To detect the bubbles evolving at the microelectrode by means of overpotential or impedance fluctuations, the size of the electrode's active area must be comparable to the bubble size. The active area of the microelectrodes used during the experiments was determined by the SiO_2 , Si_3N_4 , polyimide window $60 \times 60 \mu\text{m}^2$ square. It should be noted that the polyimide cannot be directly deposited on the electrode metal due to its ability to redox reactions in

electrolyte solutions.⁽¹⁶⁾ The SiO₂, Si₃N₄ layers were included to avoid this problem. The wafers were then cut into pieces and the chips were mounted on 8 × 100 mm² printed circuit board carriers and then encapsulated in epoxy resin.

3.2 Gas bubble detection and measurement set-up

The MCEs were used as cathodes, and hydrogen bubbles were produced according to the hydrogen evolution reaction (in alkaline medium):



The MCEs were used as working electrodes in the setup schematically presented in Fig. 6. A platinum plate with a much bigger area than the working electrode (approx. 1 cm²) was used as a counterelectrode. A voltage-controlled current source connected the working electrode and the counterelectrode. The overpotential and impedance fluctuations were measured between the working electrode (WE) and a calomel reference electrode (RE). The instrumentation amplifier was designed with two channels to allow simultaneous measurement of the overpotential and impedance fluctuations due to bubble evolution. The overpotential channel automatically removed the mean value of the potential measured between the RE and the WE, making it possible to monitor only the ac fluctuations around this mean value. This was achieved with the DC-shift block and a low-pass filter. For the impedance measurements, a signal (ACin) with a frequency of 100 kHz and a small amplitude (typically 50 mVpp) was added to the control voltage of the current source (DCin) by means of a summing amplifier Σ. The frequency of the small signal was high enough to ensure that the electrode impedance was measured. The same frequency was also used previously.⁽¹¹⁾ The amplitude of this small signal voltage was chosen such that the fluctuations in the resulting current from the current source could also be consid-

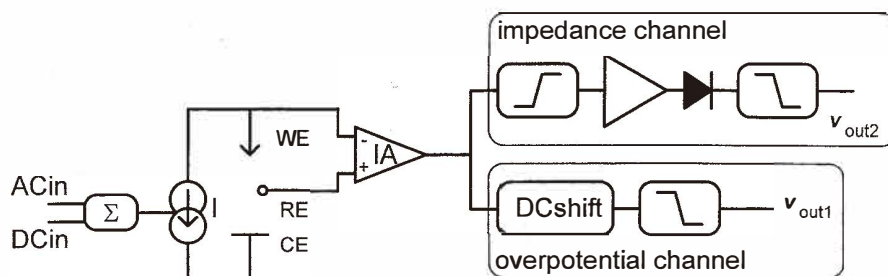


Fig. 6. Measurement setup. WE is the working electrode, CE is the counterelectrode, RE is the reference electrode. I is the electrolysis current of a voltage-controlled current source. ACin and DCin are the control voltages applied to the current source by means of the summing amplifier Σ. v_{out1} corresponds to the measured overpotential and v_{out2} corresponds to the measured impedance fluctuations. IA is the instrumentation amplifier.

ered small signals with respect to the DC value applied for the electrolysis. The impedance channel consisted of a high-pass filter, an amplifier, a demodulator and a low-pass filter. No phase difference could be measured between the two channels of the amplifier. The experiments were performed in 10 mM sodium acetate (NaAc, Merck, analytical grade) or sodium sulfate (Na_2SO_4 , Merck, analytical grade) solutions with different surfactant concentrations (nonionic surfactant, Synperonic NP9, courtesy of Unilever). The solution pH was 7.4. All the experiments were carried out at room temperature (20°C).

Optical monitoring of bubble evolution was performed using a Volpi TV Modular Microprobe system and a miniature CCD color camera (Teli, type CS5131) connected to a video recorder. An external light source (Intralux 6000-1) was used in addition to the internal light source of the microsonde (Intralux 6000-1). The magnification of the optical system was about $\times 400$.

4. Results

4.1 *Restrictions to the model of the concentrator effect*

It should be emphasised that the analytical model presented in this paper is intended to explain why bubble nucleation occurs on the bottom of the cavities and not elsewhere on the electrode surface. No predictions of any kind can be made on the basis of this model after the appearance of the gas phase on the bottom of the cavity. The assumption that the current is uniformly distributed over the whole electrode area is certainly not valid after this point.

In the simplified three-dimensional analytical model presented in this paper, it is assumed that there are three semi-infinite electrodes perpendicular to each other. In reality, the electrodes are finite and embedded in a plane electrode with limited dimensions (Fig. 1). Fringing effects will occur at the intersection of the plane in which the cavity is embedded and at the side walls of the cavity due to diffusional transport parallel to the electrode. If the cavity is deep enough, these fringing effects will have no influence on the concentration profile on the bottom of the cavity if the current is assumed to be uniformly distributed. The difference between the concentration on the bottom and at the edge will be larger in reality than in the simulated situation and therefore a bubble is more likely to nucleate on the bottom of the cavity.

The MCEs are produced in silicon by means of anisotropic etching and other planar technologies. The resulting shape is a reversed pyramid with a square base embedded in a plane. The pyramid has four side walls contributing to the concentration profile instead of the modelled three wall configuration. The three wall configuration was dictated by the analytical approach used in the model. It is likely that the concentration of gas on the bottom of the cavity will again be higher in reality than in the case of the three electrodes perpendicular to one another, since the actual cavity is deeper than that modelled by a factor of 1.14 for the same lateral cavity area. This means that the concentration difference between the bottom of the cavity and its mouth will be even greater and that the concentrator effect will still occur. It should be noted that this simple analytical model can provide first-order theoretical support to the concept of microelectrode surface shaping for batch

manufacturing of reproducible single-nucleation site electrodes. Although a more accurate model could be more appropriate, this analytical model still supports the concept of electrode surface shaping for the fabrication of reproducible single nucleation sites.

4.2 Overpotential and impedance recordings

Simultaneous measurement results of the overpotential and impedance fluctuations at MCEs are presented in Figs. 7(a) and 7(b). The periodic nature of bubble evolution and of nucleation can be seen in Fig. 7(a), supporting the idea of controlled heterogeneous nucleation on the bottom of the cavity. The same periodic character was observed with the optical system. It was obvious that the bubbles nucleated on the bottom of the cavity. Fig. 7(b) presents the fluctuations of the waveform over one period (nucleation and growth of one bubble). It can be seen that the shape of the fluctuations is different at the output of the overpotential and of the impedance channels. Different shapes of the overpotential and impedance fluctuations were also observed previously,⁽¹¹⁾ but for several bubbles evolving at the same time. No correlation between the two recordings published in ref. 11 is possible.

When only one bubble is evolving on the electrode, a qualitative interpretation of the measured waveforms of overpotential and impedance becomes possible. It has already been mentioned that the MCE working electrodes were used as cathodes. That means that during the electrolysis of water, these electrodes should become more negative with respect to the reference electrode. The measurement circuitry detects the absolute value of the fluctuations of the working electrode potential (fluctuations of the overpotential) with respect to this reference electrode, which means that, when the working electrode becomes more negative, the measured signal at the output of the overpotential channel reaches more positive values.

When one bubble has nucleated in the cavity, an increasing part of the electrode surface is shielded by it and the impedance of the working electrode increases. Also the overpotential becomes more negative and thus the absolute value of the overpotential fluctuations becomes more positive. The initial steep slope of this overpotential variation can be due to additional effects such as the stirring effect of the moving bubble interface and variations in the concentration overpotential. When the absolute value of the overpotential has reached a maximum, it then starts to decrease. The results published in ref. 10 do not show a decrease in the overpotential during the bubble growth stage. This might be because Gabrielli *et al.*⁽¹⁰⁾ used flat disk microelectrodes. The concentration profile in the case of a disk electrode is different from those obtained on MCEs and is certainly less steep. The overpotential decrease observed in Fig. 7(b) may be due to the fact that the concentration overpotential due to dissolved gas decreases since the dissolved gas is taken up by the gas bubble at a higher rate than it is generated by electrolysis. It is possible that such a regime can only be observed on microelectrodes with surface shaping, such as the MCEs. This assumption is supported by the observation that the impedance of the MCE increases faster at the end of the bubble growth stage, which may be due to a fast increase of the shielded electrode area due to faster bubble growth. Simulation results presented in ref. 12 indicate the possibility that the cathode potential becomes less negative (decrease in the absolute value) when the bubble growing on the electrode takes up more gas from the solution than

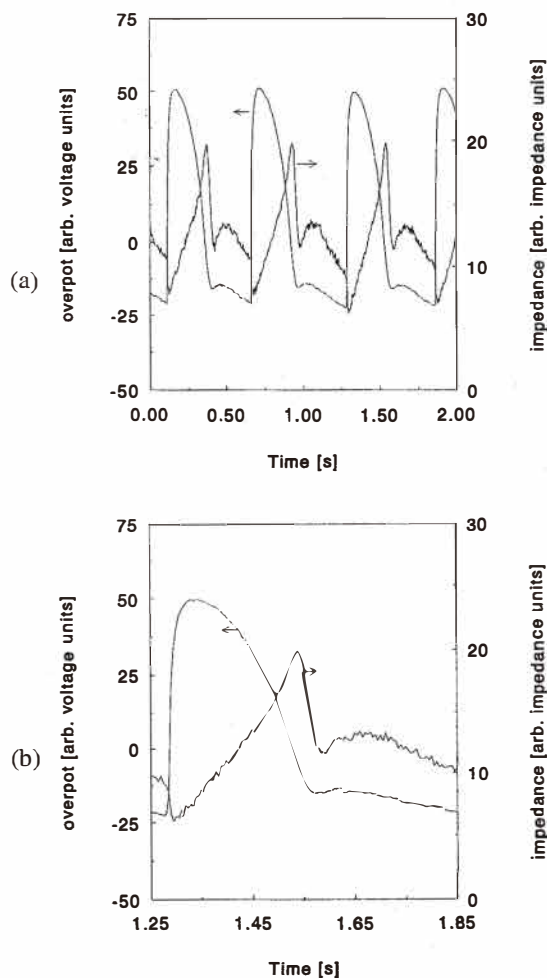


Fig. 7. Measured fluctuations of the overpotential and impedance fluctuations at MCEs during periodic bubble evolution. (a) Periodic evolution. (b) Detail of one period. Measurements in 10 mM NaAc with 0.8 g/l nonionic surfactant (Synperonic NP9). The estimated bubble frequency is 0.56 Hz at an electrolysis current of $5.93 \mu\text{A}$.

is produced by electrolysis, because the concentration overpotential at the cathode becomes less negative.

When the bubble reaches its detachment condition, the surface tension that keeps the bubble on the electrode becomes equal to the buoyancy that acts vertically upwards on the bubble. For the inclined walls of the cavity, this means that the surface tension has a

component in the vertical direction. This vertical component contributes to the force balance at the bubble detachment moment. Although the polyimide is in contact with the electrolyte, its margin is far enough from the cavity that it does not influence the detachment process as observed under the microscope. The detachment moment is seen on the impedance recording since the impedance drops very sharply at this point.

After the bubble detachment, the whole electrode area is again in contact with the solution. This situation remains unchanged until a new bubble nucleates in the cavity. This is the time at which the supersaturation needed for the nucleation of a new bubble is again reached on the bottom of the cavity and is dependent on the rate at which gas is produced at the microelectrode, i.e., on the electrolysis current density. A higher gas production rate, corresponding to a higher current density, will give a shorter time interval before a new bubble nucleates at the electrode. The effect of the current density can be seen in Fig. 8, where recordings of the bubble frequency at three current values are presented.

The second peak that is observed on both the overpotential and the impedance registrations (Fig. 7(b)) has another explanation. The local stirring caused by the detachment and the rise of the gas bubble brings solution with a different composition into contact with the electrode. This phenomenon may explain the origin of the peak, and it is supported by the observation that the measurements are very sensitive to movements in the solution. Sensitivity to movements is expected because the whole electrolysis process is mass-transfer controlled.

It has already been mentioned that the surface tension of the solution plays an important

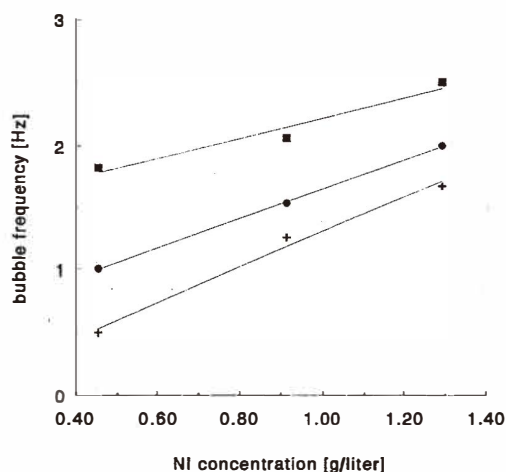


Fig. 8. Measured dependence of the bubble frequency on the surfactant concentration (dynamic surface tension) at various electrolysis currents. Measurements in 10mM Na_2SO_4 and with various concentrations of nonionic surfactant (Synperonic NP9). The electrolysis current is ■ 6 μA ; ● 5.3 μA ; + 4.8 μA .

role in bubble detachment. It is typical to investigate the influence of the surface tension of the solution on the evolution of gas bubbles at MCEs. To this end, the frequency of the periodical process of bubble evolution is a good measurable parameter. This frequency can be determined from the recordings of either the overpotential or the impedance fluctuations. Due to the controlled periodical nucleation, spectral analysis described in ref. 7 is not necessary. The results presented in Fig. 8 show that the bubble frequency is a monotonic function of the surfactant concentration (surface tension) at a constant electrolysis current; the higher the surfactant concentration, the higher the bubble frequency. This indicates that the MCE device can be used as a sensor for monitoring the surface tension in aqueous solutions. The use of MCEs as sensors is interesting because of their reduced size. Additionally, the bulky gas compressors that are usually needed for measurements based on sparging (i.e., blowing gas with a constant flow through a tube into the solution) can be replaced in this case with a relatively simple current source to generate gas with a constant rate by electrolysis. The disadvantage is that an aqueous solution is needed for the electrolysis, which limits the applicability of the sensor.

As already mentioned, the bubble detachment condition requires that the surface tension that keeps the bubble attached to the electrode be equal to the buoyancy that tends to detach the bubble. The surface tension depends on the surfactant concentration in such a way that the higher the surfactant concentration, the lower the surface tension. A lower surface tension also means that the bubble detachment condition is satisfied for smaller bubbles. If the gas production rate by electrolysis is kept constant by keeping the electrolysis current constant, a higher bubble frequency and smaller bubbles will be observed for decreasing surface tension, just like in Fig. 8.

Comparative measurements of the bubble frequency at different concentrations of nonionic surfactant (Synperonic NP9) and in 10 mM solutions of NaAc and Na₂SO₄ are given in Fig. 9. It appears that not only the changes in the surfactant concentration but also the type of background electrolyte influence the bubble frequency. The bubble frequency is lower in the NaAc solution. The difference in the conductivity of the two solutions cannot explain this difference because the measurements are performed at constant current. The difference may be due to differing surface tensions of the two salt solutions.

Other liquid properties such as viscosity and density could also, in principle, influence the bubble evolution process. However, the variation in these parameters is very small in aqueous solutions and was not further investigated in this paper.

5. Discussion

We conclude that controlled gas bubble formation during electrolysis by means of electrode surface shaping in the form of MCEs is possible. A reversed pyramid shape was chosen for this purpose. A simplified theoretical model was given to support the concept of electrode surface shaping for reproducible nucleation of gas bubbles. The cavity functions as a gas concentrator producing a higher concentration of dissolved gas on the bottom of the cavity than anywhere else in the solution before the nucleation of a bubble takes place. The chance of heterogeneous nucleation of a bubble occurring on the bottom of the cavity

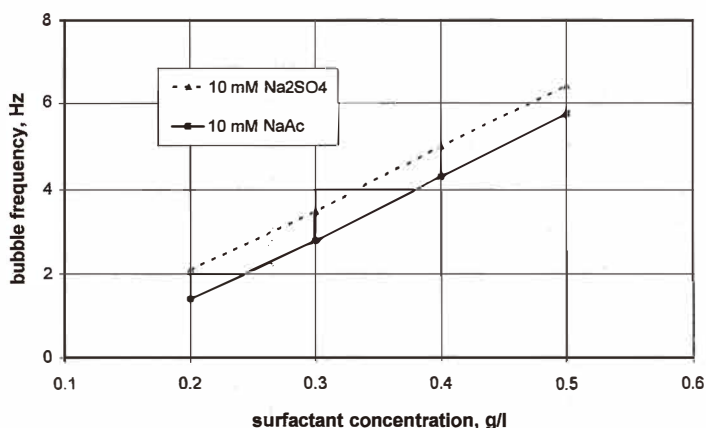


Fig. 9. Measurements of the surfactant concentration effect with 10 mM NaAc or Na₂SO₄ background electrolyte. Electrolysis current was 5.63 μ A.

is thus much higher. The MCE fabrication process uses planar batch processing technology with all its advantages in terms of reproducibility.

The experimental results proved the possibility of generating reproducible monosized gas bubbles by means of electrolysis at MCEs. The detection of the bubble evolution process was performed by means of simultaneous measurement of the overpotential and the impedance fluctuations. The recorded waveforms showed that the gas bubble evolution has a constant bubble frequency. A qualitative explanation of the measured waveforms was proposed based on the phenomena that take place at the electrode during electrolysis. By monitoring the bubble frequency, the influence of the surface tension and of the electrolysis current on the bubble evolution were investigated. The possibility of using the MCE electrode as a surface tension sensor with a frequency output was recognized.

Acknowledgments

The research is financially supported by Unilever.

The authors wish to thank Ir. Dion Oudejans who fabricated the MCE devices used in the experiments.

Appendix

It can be shown that the solution of eq. (9) (eq. (A1)) satisfies the diffusion equation (1) and the initial and boundary conditions (2)–(6).

$$C(x, y, z, t) = k \left(2\sqrt{\frac{Dt}{\pi}} \exp\left(\frac{-x^2}{4Dt}\right) - x \cdot \operatorname{erfc}\left(\frac{x}{2\sqrt{Dt}}\right) \right) + k \left(2\sqrt{\frac{Dt}{\pi}} \exp\left(\frac{-y^2}{4Dt}\right) - y \cdot \operatorname{erfc}\left(\frac{y}{2\sqrt{Dt}}\right) \right) + k \left(2\sqrt{\frac{Dt}{\pi}} \exp\left(\frac{-z^2}{4Dt}\right) - z \cdot \operatorname{erfc}\left(\frac{z}{2\sqrt{Dt}}\right) \right) \quad (\text{A1})$$

The diffusion equation and the initial and boundary conditions are repeated below.

$$\frac{\partial C(x, y, z, t)}{\partial t} = D \left(\frac{\partial^2 C(x, y, z, t)}{\partial x^2} + \frac{\partial^2 C(x, y, z, t)}{\partial y^2} + \frac{\partial^2 C(x, y, z, t)}{\partial z^2} \right) \quad (\text{A2})$$

$$x, y, z \geq 0$$

$$\frac{\partial C(0, y, z, t)}{\partial x} = -\frac{J}{nDF} = -k \quad (\text{A3})$$

$$\frac{\partial C(x, 0, z, t)}{\partial y} = -\frac{J}{nDF} = -k \quad (\text{A4})$$

$$\frac{\partial C(x, y, 0, t)}{\partial z} = -\frac{J}{nDF} = -k \quad (\text{A5})$$

$$C(x, y, z, 0) = 0, \quad x, y, z > 0 \quad (\text{A6})$$

$$\lim_{x, y, z \rightarrow \infty} C(x, y, z, t) = 0, \quad t > 0 \quad (\text{A7})$$

A simple substitution of the solution (A1) into eqs. (A6) and (A7) shows that these conditions are satisfied. For a further demonstration, the spatial and temporal derivatives of the point concentration (eq. (A1)) are needed.

$$\frac{\partial C}{\partial x} = -k \cdot \operatorname{erfc}\left(\frac{x}{2\sqrt{Dt}}\right) \quad (\text{A8})$$

$$\frac{\partial C}{\partial y} = -k \cdot \operatorname{erfc}\left(\frac{y}{2\sqrt{Dt}}\right) \quad (\text{A9})$$

$$\frac{\partial C}{\partial z} = -k \cdot \operatorname{erfc}\left(\frac{z}{2\sqrt{Dt}}\right) \quad (\text{A10})$$

$$\frac{\partial C}{\partial t} = k \left[\sqrt{\frac{D}{\pi t}} \left(\exp\left(\frac{-x^2}{4Dt}\right) + \exp\left(\frac{-y^2}{4Dt}\right) + \exp\left(\frac{-z^2}{4Dt}\right) \right) \right] \quad (\text{A11})$$

Substitution of $x = 0$, $y = 0$ and $z = 0$ into eqs. (A8), (A9) and (A10), respectively, shows that the boundary conditions (A3)–(A5) are also satisfied.

Furthermore,

$$\frac{\partial^2 C}{\partial x^2} = \frac{k}{\sqrt{\pi Dt}} \exp\left(\frac{-x^2}{4Dt}\right) \quad (\text{A12})$$

$$\frac{\partial^2 C}{\partial y^2} = \frac{k}{\sqrt{\pi Dt}} \exp\left(\frac{-y^2}{4Dt}\right) \quad (\text{A13})$$

$$\frac{\partial^2 C}{\partial z^2} = \frac{k}{\sqrt{\pi Dt}} \exp\left(\frac{-z^2}{4Dt}\right), \quad (\text{A14})$$

and the diffusion equation (A2) is also satisfied.

References

- 1 H. Vogt: *Electrochim. Acta*, **38–10** (1993) 1427.
- 2 H. Vogt: *Electrochim. Acta*, **38–10** (1993) 1421.
- 3 C. W. M. P. Sillen: Ph.D. Dissertation, University of Eindhoven (1983).
- 4 A. Volanschi, W. Olthuis and P. Bergveld: *Proceedings of Transducers '95 and Eurosensors IX*, Stockholm, Sweden (1995).
- 5 A. K. Chesters: *Bubble Sizes in Nucleate Pool Boiling*, in *Boiling Phenomena*, eds. S. Stralen and M. Cole (McGraw Hill Book Company, 1979) 879.
- 6 A. Sahar: Ph.D. Dissertation, University of Paris, VI (1988).
- 7 C. Gabrielli, F. Huet, M. Keddam and A. Sahar: *J. Appl. Electrochem.* **19** (1989) 683.
- 8 S. D. Lubetkin: *Controlled Particle, Droplet and Bubble Formation*, ed. D. J. Wedlock (Butherworth & Heinemann, 1994) p. 159.
- 9 D. E. Westerheide and J. W. Westwater: *AIChE Journal* **7–3** (1961) 357.
- 10 C. Gabrielli, F. Huet, M. Keddam, A. Macias and A. Sahar: *J. Appl. Electrochem.* **19** (1989) 617.
- 11 C. Gabrielli, F. Huet and M. Keddam: *J. Electrochem. Soc.* **138–12** (1991) L82.
- 12 J. Dukovic and C. W. Tobias: *J. Electrochem. Soc.* **134–2** (1987) 331.
- 13 J. L. Leistra and P. J. Sides: *J. Electrochem. Soc.* **134** (1987) 2442.
- 14 H. S. Carslaw and J. C. Jaeger: *Conduction of Heat in Solids*, Oxford University press (1959).
- 15 A. V. Luikov: *Analytical Heat Diffusion Theory* (Academic Press) (1968).
- 16 S. M. Lian, K. M. Chen and A. Hung: *J. Electrochem. Soc.* **141–9** (1994) 2374.